

Isomeric states in neutron-rich $Z = 76$ isotopes and $N = 116$ isotonesA. Kardan ¹, P. M. Walker ², and I. Ragnarsson ³¹*School of Physics, Damghan University, P.O.Box 36716-41167, Damghan, Iran*²*Department of Physics, University of Surrey, Guildford GU2 7XH, United Kingdom*³*Division of Mathematical Physics, LTH, Lund University, Box 118, SE-221 00 Lund, Sweden*

(Received 21 November 2023; accepted 1 March 2024; published 28 March 2024)

We have employed both unpaired (cranked Nilsson-Strutinsky) and paired (cranked Nilsson-Strutinsky-Bogoliubov) cranked Nilsson-Strutinsky calculations to explore the properties of observed and potential isomers within the shape-transitional osmium ($Z = 76$) isotopes and $N = 116$ isotones. Our analyses reveal the prevalence of multiquasiparticle prolate and broken-pair triaxial structures in even-even osmium isotopes ($N = 112$ – 118) and $N = 116$ isotones ($Z = 72$ – 80). In addition, our exploration of $N = 116$ isotones identifies potential isomeric states, systematically, including noncollective 10^- and collective 12^+ states, constructed upon specific neutron configurations.

DOI: [10.1103/PhysRevC.109.034320](https://doi.org/10.1103/PhysRevC.109.034320)**I. INTRODUCTION**

Nuclear isomers, with their unique configurations and distinct quantum states, have garnered significant attention in the field of nuclear physics. Isomers are excited nuclear states which have a relatively long lifetime on the nuclear timescale, sometimes longer than their ground states, making them intriguing subjects for investigation [1]. Their study not only sheds light on the fundamental properties of atomic nuclei but also holds promise for various applications in areas such as nuclear astrophysics, medical imaging, energy storage, and superaccurate time keeping [2,3].

The understanding of nuclear isomers and their characteristics has undergone significant advancement in recent years in experimental techniques and theoretical models [3]. These tools have enabled researchers to probe the structure, formation mechanisms, and decay properties of isomers with remarkable precision and depth [1,3,4]. As the isomer data grew in number, they gradually began to play a crucial role in the development of various nuclear models [5]. Numerous studies based on nuclear models, such as the nuclear shell model [6,7], and mean-field approaches [8–10], have provided valuable insights into the formation and behavior of isomers. For example, theoretical calculations have elucidated the role of shape coexistence, deformation, and collective excitations in stabilizing isomeric states in certain nuclei [11,12]. Furthermore, theoretical studies have revealed intriguing phenomena associated with nuclear isomers, such as shape isomerism and spin traps [4]. Shape isomerism occurs when the nuclear potential-energy landscape exhibits multiple minima corresponding to different shapes, leading to the coexistence of different isomeric states with distinct structures [12].

Research findings indicate a robust link between the presence of isomers and the placement of intruder orbitals relative to the Fermi surface [13]. These unique-parity intruder orbitals carry large angular momentum and opposite parity,

leading to high-spin excitations at low energy. These conditions support a hindered transition, and formation of isomers. Numerous K -isomers have been detected in deformed nuclei, particularly in nuclei with atomic masses around 130 and 180, as the high- j orbitals are situated close to the Fermi surface within these mass regions, resulting in substantial angular-momentum projections. Certain combinations of Nilsson orbitals emerge in various multiquasiparticle (MQP) states. These combinations of Nilsson orbitals appear in the MQP configurations as fundamental constituents for numerous isomeric states [14]. Accurate calculations of MQP energies remain a challenging task due to the involvement of multiple factors, requiring a comprehensive understanding of the nuclear shape, the single-particle energies, the pairing energy, and the residual nucleon-nucleon interaction energy.

In the $A \approx 180$ – 190 region, also collective oblate or close to oblate isomers have been predicted and possibly observed at high spin [15–17]. A long lifetime, via a single transition, results from a small transition energy or a profound change in quantum numbers or/and nuclear structure within the isomer and the state to which it decays [18]. For collective isomers, long lifetimes result mainly from small transition energies, see collective isomers in Refs. [17,19]. Recent theoretical investigations have explored gamma-vibrations, static triaxiality, and mean-field calculations aiming to describe the shape evolution of ground and excited states across a wide range of neutron-rich Hf, W, Os, and Pt nuclei [20–23]. Isomeric states typically dominate the collective configurations in this region, such as the long-lived 12^+ states in even- A Pt isotopes [19,24]. Studies show these 12^+ isomeric states result from the rotation alignment of a pair of $i_{13/2}$ neutrons [15,25]. According to configuration-constrained potential-energy-surface calculations, additional prolate and triaxial structures are predicted in Os isotopes [17]. However, there is limited information available on these structures. These predicted states in Os isotopes, along with similar ones in iridium nuclei [26], pose a

challenge for future experimental studies and the understanding of shape variations and competing dynamics in transitional nuclei.

The main goal in the present theoretical work is to identify yrast states and to search for the collective and noncollective potential isomers in even-even osmium isotopes, particularly focusing on the heaviest stable Os isotope, ^{192}Os . The study aims to examine the evolution of collectivity with increasing neutron number. Our study additionally delves into a systematic exploration of energetically favored MQP states within the $N = 116$ isotones, with a focus on two critical neutron structures. This study provides valuable insights into structure and behavior, contributing to a deeper understanding of favored states in the corresponding mass region.

II. THEORETICAL FRAMEWORKS

Calculations have been carried out in the paired cranked Nilsson-Strutinsky-Bogoliubov (CNSB) and unpaired cranked Nilsson-Strutinsky (CNS) formalisms. The CNS model is defined in Refs. [27,28] and the CNSB model which is based on the ultimate cranker [29], is defined in Refs. [30,31]. In these cranking models, the rotation degree of freedom enters in the same way as the deformation degree of freedom. In the CNS and CNSB models, the Lublin Strasbourg Drop (LSD) model [32], accounts for the macroscopic part of the energy and the Strutinsky shell correction [33], based on the Nilsson single-particle potential, is used for its microscopic part. The total energy of the nucleus is minimized by finding the optimal values for the deformation parameters, ε_2 , γ , and ε_4 , in the CNS model, and for the deformation and pairing parameters, the pairing gap Δ and the Fermi energy λ , in the CNSB, at each spin. The Fermi energy, λ which is the Lagrange multiplier in the Bogoliubov equations, ensures that the expectation value of the particle number operator is conserved, see, for example, Ref. [34]. The angle γ is introduced in such a way that axial symmetry is preserved when $\gamma = -120^\circ$, -60° , 0° , or 60° . All ellipsoidal shapes can be described within one 60° sector, but the rotation occurs around the shortest, the intermediate, and the longest principal axis for $\gamma = [0^\circ, 60^\circ]$, $\gamma = [0^\circ, -60^\circ]$, and $\gamma = [-60^\circ, -120^\circ]$, respectively.

The only difference between the CNS and the CNSB yrast configurations is the pairing energy. The exclusion of pairing, combined with the simplicity of the Nilsson (modified oscillator) potential makes it possible to fix the structure of configurations in the CNS procedure, see Ref. [35]. However, utilizing the CNS formalism at lower angular momenta, where neglecting pairing exposes significant deviations of especially calculated energies, becomes questionable. In contrast, the inclusion of pairing correlations within the CNSB formalism proves successful in replicating additional properties, especially those associated with isomers frequently observed at lower angular momenta, see Ref. [10].

In both CNS and CNSB formalisms, a ‘‘adiabatic’’ technique is utilized to obtain wave functions with a smooth dependence on Hamiltonian parameters [29]. This method offers a notable advantage, enabling the presentation of results as a function of spin rather than rotational frequency [27,36]. This

stands in contrast with models, where results are presented based on rotational frequency, an experimentally unmeasurable parameter. In CNSB calculations, the pairing strength G is determined by solving the unified model [29]. In the present calculations, the G value is adjusted with a reduction of 2%–5%. It is based on studies indicating that particle number projection tends to produce a larger pairing correlation than BCS calculations [36,37]. Our reduction might be somewhat small but the exact value will not be important for our conclusions.

The single-particle parameters are the standard parameters modified for Hf region [38].

III. FAVORED NONCOLLECTIVE MQP STATES IN $Z = 76$ ISOTOPES

In Fig. 1, we have drawn the neutron and proton single-particle energies. Let us first consider the three high- K 2 quasineutron (qn) states: the 12^+ state built on two $i_{13/2}$ neutrons with $\Omega = 13/2$ and $11/2$, crossing at $\hbar\omega \approx 0.2$ MeV, and the 6^+ state built on two $9/2[505]$, $3/2[512]$ neutrons and 8^+ built on two $9/2[505]$, $7/2[503]$ neutrons, i.e., the highest possible spin which can be built within the hf neutrons, see Fig. 1(b). Then two 4-qn high- K 18^+ and 20^+ states can be formed by combination of the 12^+ state with the 6^+ and 8^+ states. Also we find a 2-quasiproton (qp) high- K state in the proton energy diagram in Fig. 1(a) where two $h_{11/2}(\Omega = 11/2, 9/2)$ orbitals cross at $\hbar\omega \approx 0.2$ MeV and build a 10^+ state which is favored in energy. Thus, we also have a 4-quasiparticle 22^+ state ($=10_p + 12_n$) and a 6-quasiparticle 28^+ state ($=10_p + 18_n$). All these states are obtained by searching only among the $(\pi, \alpha)_p(\pi, \alpha)_n = (+, 0)(+, 0)$ configurations.

We have also looked into the paired single-particle energies calculated in the CNSB framework. We find the 10^+ proton and 12^+ neutron states built at a similar crossing at $\hbar\omega \approx 0.25$ MeV to that of the unpaired calculations. The 6^+ state is also seen in the paired calculations but at much higher frequency ≈ 0.3 MeV while the 8^+ crossing is slightly closer to the Fermi level. It shows that the 18^+ and 20^+ states become more favored if the pairing interaction is included in the calculations.

Figure 1(b) also shows the known 10^- state, which is constructed based on the $11/2[615]9/2[505]$ neutron configuration. The $11/2[615]$ and $9/2[505]$ crossing occurs at $\hbar\omega \approx 0.2$ MeV in the (paired) quasiparticle energies. Also, this crossing is identified very close to the Fermi level (≈ 0.08 MeV) in the paired calculations, making it likely to be observable in experiments. We revisit this state in Sec. V with further discussion.

A. Favored states in ^{192}Os

The potential-energy surfaces of the CNSB calculations are drawn in Fig. 2 for the selected $(\pi, \alpha)_p(\pi, \alpha)_n = (+, 0)(+, 0)$ configurations. The calculations predict a prolate but γ -soft potential minimum for the ground state. There is a triaxial minimum at $\gamma \approx -90^\circ$ which becomes yrast or close to yrast at $I = 12^+$, 18^+ , 20^+ , and 22^+ . A fixed deformation calculation can show these competing states better. In Fig. 3, energy

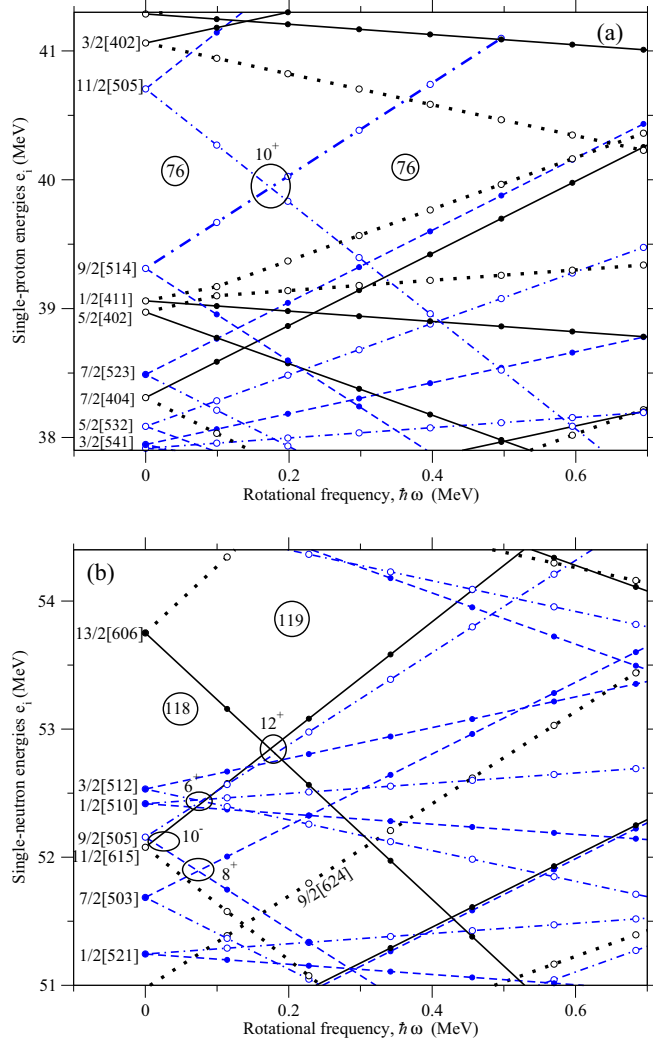


FIG. 1. Unpaired CNS single-particle Routhians for (a) protons and (b) neutrons for the deformation $\varepsilon_2 = 0.143$, $\varepsilon_4 = 0.041$, and $\gamma = -120^\circ$. The line types distinguish between different (π, α) combinations: solid lines represent $(+, +1/2)$, dotted lines $(+, -1/2)$, dashed lines $(-, +1/2)$, and dash-dotted lines $(-, -1/2)$. A few important crossings for the present interpretation are highlighted.

versus spin for different shapes is shown. As seen in Fig. 2, the γ value for the collective prolate minimum is changed from zero to around -30° at $I = 0-12$. Therefore, we have done the calculation with a minimization starting from the collective prolate $\gamma = 0^\circ$ point so that γ value can change to $\gamma \approx -30^\circ$. There are no minimum calculated at collective oblate shape and the high energy of this curve suggests that there are no oblate configurations in the yrast region of ^{192}Os for $I \lesssim 30$. We can see that there is a competition between collective prolate, noncollective prolate, and triaxial states at low spins. Also it is seen that there is a strong competition between noncollective prolate states and triaxial states around $I = 12^+$ and around $I = 22^+$. It shows that the MQP $I = 10^+$, 12^+ , and the 22^+ states are disturbed by the triaxial states while the noncollective $I = 18^+$ state is lower than the triaxial one by around 1 MeV. The current calculations show that the triaxial

minima appear at $I > 24$ for $(+, 0)(-, 0)$ configurations so that there is not such a competition between the noncollective and collective states at lower spin for negative-parity configurations.

Table I shows the configuration assigned to each of the calculated high- K MQP states in ^{192}Os and their energy. The deformation in these configurations is $\varepsilon_2 \approx 0.14$, $\gamma = -120^\circ$, $\varepsilon_4 \approx 0.04$. Note that those are yrast except for the 12^+ and 22^+ states, see Fig. 3, where triaxial states have energies 2.151 and 4.004 MeV, respectively, are yrast. This triaxial configuration is seen in the potential-energy surfaces, Fig. 2. As one can see in Fig. 1(a), there is a large single-particle shell gap associated with proton number $Z = 76$ that continues to $\hbar\omega \simeq 0.55$ MeV including the $11/2[505]$ and $9/2[514]$ crossing. It means that except for the $\pi 11/2[505]9/2[514]$ state, the other proton excitations will come higher in energy, making their observation less likely. Consequently, our study has primarily focused on the $(+, 0)(\pm, 0/1)$ configurations, as reflected in Table I. The 7^- and 17^- states are also high- K states with negative parity and favored in energy in ^{192}Os , see their energy and structure in Table I. In Pt isotopes with two protons more, the $3/2[402]$ orbital will come close to the Fermi level [see Fig. 1(a)] and then it is more likely to build the 7^- on the $11/2[505]3/2[402]$ proton structure that would be consistent with g factor measurements [19,24,25]. The measured g factor, $+0.62$, for this state in ^{190}Pt indicates a 2-qp configuration while a decreasing g factor (from $+0.48$ to -0.03) for the heavier isotopes, $^{192-196}\text{Pt}$, suggests a 2-qn $11/2[615]3/2[512]$ ($i_{13/2}, fp$) component to the configuration of the 7^- state [19]. In Hg isotopes with an additional two protons, the $3/2[402]$ is also filled, therefore the 2-qp 7^- state is no longer favored so that the 7^- state is built on the $11/2[615]3/2[512]$ neutron structure which is in agreement with the experimental g factor values [25].

The states in the Table I are written in order of increasing energy. It means the 6^+ state is the lowest 2-quasiparticle state in ^{192}Os and then the 7^- , 10^- , 10^+ , and 12^+ states. The 2-qn 8^+ ($9/2[505]7/2[503]$) state is not included in the list because it lies significantly below the Fermi level, as seen in Fig. 1(b). However, this structure contributes to the calculated 20^+ state. It is important to know that there are still some residual interactions left which have not been taken into account in the current calculations. These residual interactions result in different energies, depending on the relative orientation of the nucleon intrinsic spins. Thus, the inclusion of spin-spin interaction contributions proved important to obtain the energies and thus the correct order of states [39,40]. Based on the Gallagher-Moszkowski (GM) rule [41,42], the singlet state is the favored one in 2-quasiparticle states in even-even nuclei. Studies have shown that the GM splitting energy between triplet and singlet 2-quasiparticle states is around 300 keV in the mass-180 region [40]. It means that the two 10^- and 7^- antiparallel spin (singlet) states are favored while the other 2-quasiparticle states include two parallel spin (triplet) particles, 6^+ , 10^+ , and 12^+ , and therefore are subject to an increase in energy.

The calculation of residual interaction effects in 4- and 6-quasiparticle states is more complicated. With the assumption that the overall residual interaction in an n -

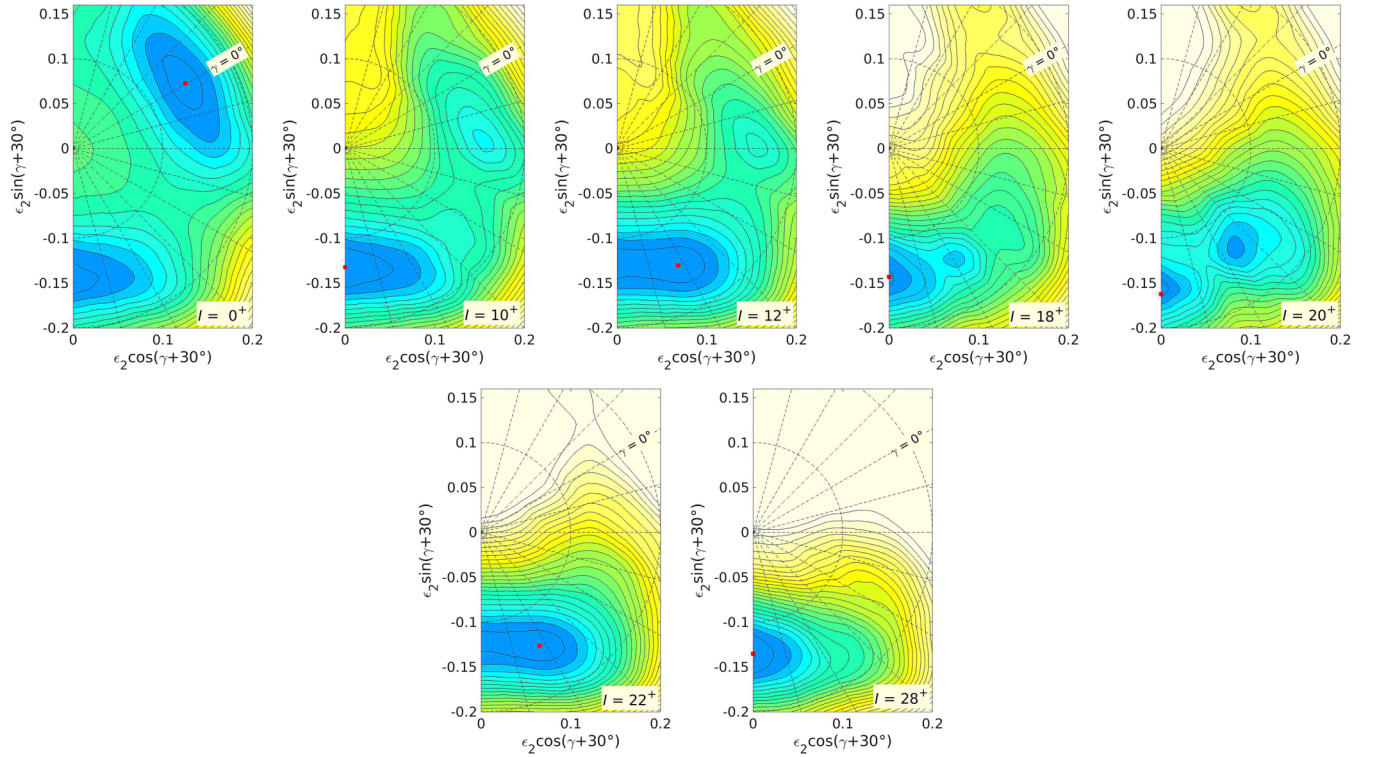


FIG. 2. Calculated CNSB potential-energy surfaces versus quadrupole deformation ε_2 and the triaxiality parameter γ of ^{192}Os for positive-parity (+, 0)(+, 0) $I = 0, 10, 12, 18, 20, 22$, and 28 states which are interpreted in the text. Contour lines are separated by 0.25 MeV and the γ plane is marked at 15° intervals. Dark regions represent low energy and absolute minima are labeled with red dots.

quasiparticle configuration is taken as the sum of the interactions between all possible 2-quasiparticle combinations, and also based on the GM rules for the neutron-neutron residual interaction [42], the 4-qn 18^+ will be favored. Since a triplet state is a favored coupling for the neutron-proton interaction [41], the 22^+ state which is built on two up-spin protons and two up-spin neutrons will be another favored candidate for 4-quasiparticle states in this nucleus. The 4-qn 20^+ and 6-quasiparticle 28^+ states are constructed from combinations of both favored and unfavored coupling pairs that are in close proximity in terms of their numbers. Therefore, they are not regarded as favored or unfavored configurations in this calculation.

B. Favored states in Os isotopes with $N = 112-118$

In the following, we study the favored MQP states as prime candidates for high- K isomers in the Os isotopes with the neutron number around $N = 116$, $^{188-194}\text{Os}$. The CNSB calculations show a prolate shape for the ground state of these isotopes with changes in γ from $\approx 0^\circ$ to $\approx -30^\circ$ for $I = 0-12$. Additionally, a general reduction in deformation is observed when neutrons are added, with a decreasing number of neutron holes below the $N = 126$ gap, from $\varepsilon_2 \simeq 0.18$ (^{188}Os) to $\varepsilon_2 \simeq 0.14$ (^{194}Os). The total Routhian surface calculations present similar deformation for $^{190-194}\text{Os}$ [43] as the current calculations while the beyond-mean-field calculations with

TABLE I. The calculated energy and structure of prolate noncollective MQP states in ^{192}Os . The energies are minimized with respect to the deformation and pairing parameters. The last column shows if the state is favored or unfavored by the Gallagher-Moszkowski rules. Energies are in MeV.

K^π	E_{calc}	Proton conf.	Neutron conf.	Coupling
6^+	1.132	GS	9/2[505]3/2[512]	Unfavored
7^-	1.417	GS	11/2[615]3/2[512]	Favored
10^-	1.538	GS	11/2[615]9/2[505]	Favored
10^+	1.814	11/2[505]9/2[514]	GS	Unfavored
12^+	2.350	GS	13/2[606]11/2[615]	Unfavored
17^-	3.396	11/2[505]9/2[514]	11/2[615]3/2[512]	Unfavored
18^+	3.426	GS	13/2[606]11/2[615]9/2[505]3/2[512]	Favored
20^+	4.176	GS	13/2[606]11/2[615]9/2[505]7/2[503]	
22^+	4.426	11/2[505]9/2[514]	13/2[606]11/2[615]	Favored
28^+	5.525	11/2[505]9/2[514]	13/2[606]11/2[615]9/2[505]3/2[512]	

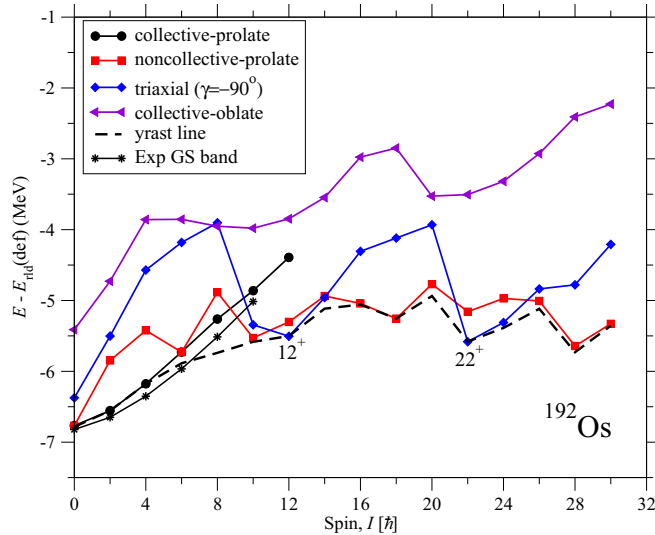


FIG. 3. The CNSB $(+, 0)(+, 0)$ yrast line in ^{192}Os compared with the energy at different fixed deformations governed by the minima shown in Fig. 2. The collective prolate state energy is obtained with a minimization starting from $\gamma = 0^\circ$. The noncollective prolate states are calculated at the deformation of the 18^+ state. Experimental ground-state energies are also shown. All energies are minimized at different pairing parameters, Δ and λ , and drawn relative to the rotating liquid drop reference.

the Gogny D1S interaction predict a shape transition from a prolate minimum ($\gamma \approx 0^\circ$) for ^{188}Os to an oblate minimum for ^{194}Os with a triaxial shape for $^{190-192}\text{Os}$ [44]. In Fig. 4, we have undertaken a comparison between the experimental ground state band and the theoretical prolate collective band for the range of $^{188-194}\text{Os}$. Remarkably, the CNSB procedure

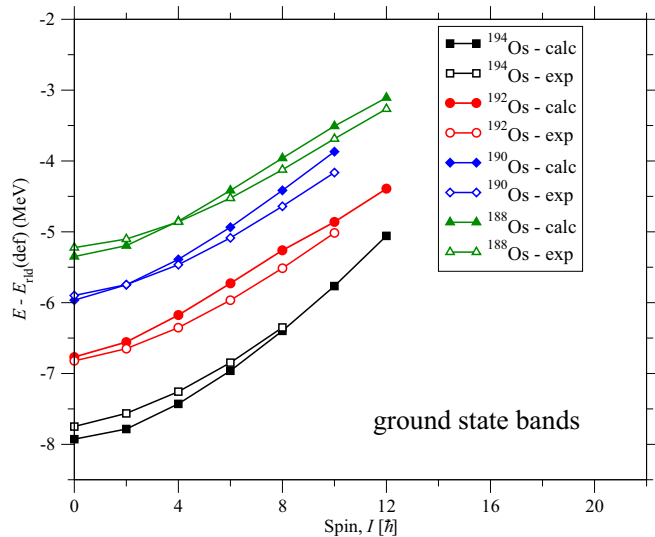


FIG. 4. Experimental and theoretical energies of the ground state bands in $^{188-194}\text{Os}$. The experimental data are taken from Ref. [45]. All energies are minimized at different deformation with a minimization starting at $\gamma = 0^\circ$ and pairing parameters, Δ and λ . Energies and drawn relative to the rotating liquid drop reference.

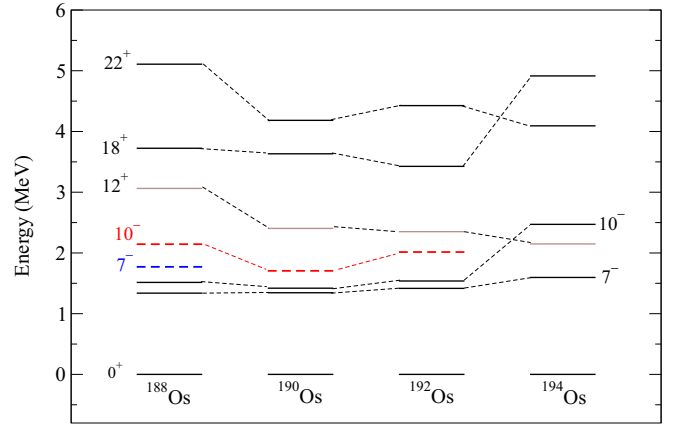


FIG. 5. The favored CNSB MQP state energies in $^{188-194}\text{Os}$ are drawn by full black lines. The unfavored 12^+ state energy is also shown in brown lines to compare with Ref. [17]. The experimental energies for 10^- isomers (in red dash lines) and 7^- isomer (in a blue dash line) are taken from Ref. [46].

effectively replicates the excitation energies observed in the ground-state bands.

The calculations in the total Routhian surface (TRS) formalism suggested that the energy of the high- K 12^+ state is expected to decrease linearly with neutron number and could fall below any state to which it could reasonably decay in ^{194}Os [17]. The energy of the related 18^+ state follows a parallel energy trajectory (see Fig. 5 of Ref. [17]). These results suggest that the 12^+ and 18^+ states would be highly populated, lying close to the yrast line. We have examined this result also in the current calculations. In the present Fig. 5, we have plotted a comparison of the energy level of the favored MQP states, detailed in Table I, alongside the predicted prolate 12^+ state in Os isotopes. The calculations show that the energy of 12^+ state decreases with increasing the neutron number. But for the 18^+ state, these calculations indicate, it is not likely to be observed in ^{194}Os because it has a higher energy than in ^{192}Os . This can be understood from Fig. 1(b) where the $9/2[505]$ is filled for $N = 118$, therefore the $h_{9/2}$ crossing will be blocked in ^{194}Os . It means the potential isomers built on the $9/2[505]$ orbital in Table I, 18^+ , 20^+ , and 28^+ will not be low in energy for ^{194}Os . As noted in Ref. [17], it is remarkable that their calculations predict (in agreement with the present work for ^{192}Os) very low-lying, high- K isomers (12^+ and 18^+) in ^{194}Os but these are not observed experimentally. It can be hypothesized that these are long-lived, beta-decaying isomers, for which experimental identification is particularly difficult—yet highly desired.

In Fig. 5, it is evident that the energy level of the 10^- state comes higher in ^{194}Os than in the lighter Os isotopes. This shift can also be attributed to the filling of the $9/2[505]$ neutron orbital within the $N = 118$ system. This observation aligns with experimental data, where the 10^- state is only observed in $^{188-192}\text{Os}$, as indicated in Ref. [46]. Additionally, Fig. 5 displays the experimental energy of the 7^- isomer which is exclusively observed in ^{188}Os . Note that our calculations suggest a similar energy of this state at least in $^{188-192}\text{Os}$, indicating the potential existence of an isomeric 7^-

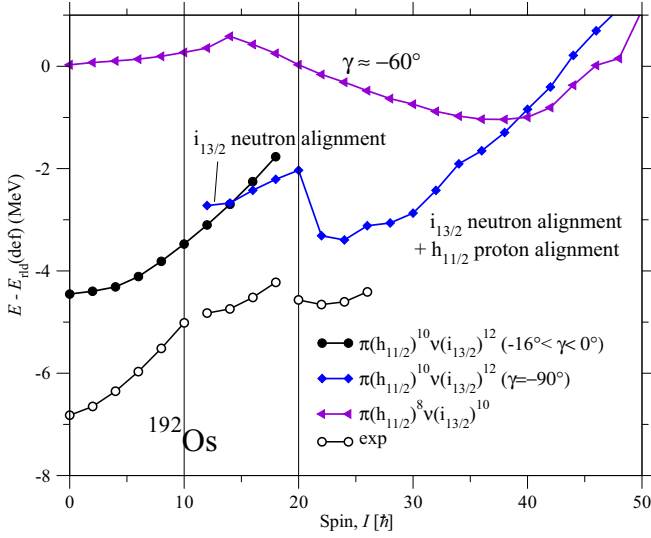


FIG. 6. The low-lying CNS $(+, 0)(+, 0)$ configurations in ^{192}Os with the collective prolate shape ($-16^\circ < \gamma < 0^\circ$), the fixed triaxial shape ($\gamma \approx -90^\circ$) and also the oblate shape. The experimental $(+, 0)$ yrast sequence energies are also drawn. The alignments in each configuration are displayed on the figure. All energies are minimized at different pairing parameters, Δ and λ , and drawn relative to the rotating liquid drop reference.

state in $^{190-194}\text{Os}$ as well. Furthermore, the 22^+ state which is favored in our calculations, displays its lowest energy in ^{194}Os , at 4.093 MeV. This characteristic suggests that ^{194}Os should be particularly favorable for the observation of this state.

It should be noted that when we compare the computation of low-lying states, we found significant differences between our results and those of the TRS calculations shown in Fig. 20 of Ref. [18]. In this section, we mainly focused on the characterization of noncollective prolate states, especially the yrast states. In contrast, Ref. [18] depicts the 10^- states of ^{188}Os and ^{194}Os and the 7^- states of ^{192}Os and ^{194}Os , among others, as exhibiting a triaxial structure, which is different from what we calculate.

IV. FAVORED COLLECTIVE STATES IN ^{192}Os

In this section, we study more deeply the structure of the lowest collective configurations within ^{192}Os . Our calculations reveal that these lowest configurations have positive parity. The CNS calculations predict that the lowest positive-parity configuration at low spin is built on $10h_{11/2}$ protons and $12i_{13/2}$ neutrons with a deformation $\varepsilon_2 \approx 0.15$ and $-16^\circ < \gamma < 0^\circ$ at $I = 0-12$, see Fig. 6. Then the neutron $i_{13/2}$ alignment will happen at $I = 12$ with a deformation change to $(\varepsilon_2, \gamma) \approx (0.15, -95^\circ)$. The total spin is then increasing regularly by rotation so that a rotational band is built on the 12^+ state. At $I = 22$, the second alignment is calculated. It is due to the $h_{11/2}$ protons and a rotational band on the 22^+ state is built with more collectivity at $\gamma \approx -90^\circ$. The crossings at $I = 12$ and $I = 22$ are because of alignment of an $i_{13/2}$ neutron pair and a $h_{11/2}$ proton pair, respectively.

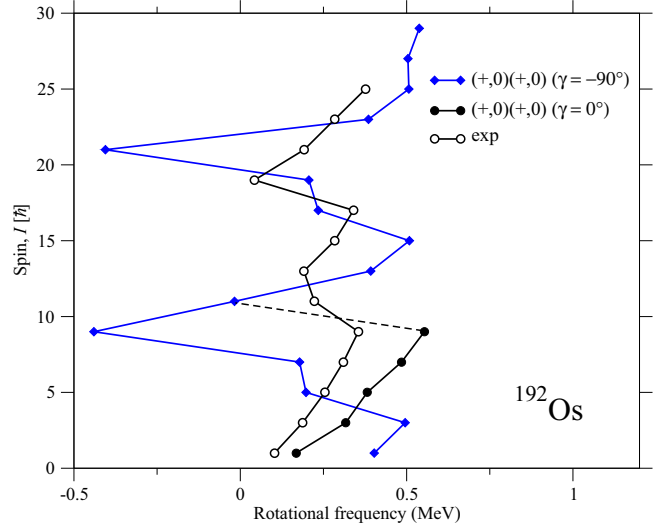


FIG. 7. Spin I versus rotational frequency $\hbar\omega$ for the experimental yrast sequence are compared with calculations for the $(+, 0)(+, 0)$ CNSB configurations with $\gamma = -90^\circ$ and $\gamma = 0^\circ$.

Comparison with experiment in Fig. 6 shows that the unpaired CNS calculations reproduce most of the energy of states well with a shift down in energy by ≈ 2 MeV. After the second alignment, where the pairing correlations become weaker, the calculated energy more closely matches experimental results, deviating by only about 1 MeV. The fact that calculations and experiment rather diverge at smaller frequencies is caused by increasing pairing correlations in the experimental data. Furthermore, Fig. 6 illustrates that the $\gamma \approx -60^\circ$ configuration $\pi(h_{11/2})^8\nu(i_{13/2})^{10}$ is favored for $I > 40$.

One can also see the collective bands built on the 12^+ and 22^+ states in Fig. 3, obtained by the CNSB approach. These results suggest that the 12^+ and 22^+ states are likely to serve as the bandhead states for the collective bands observed in ^{192}Os . However, it is seen that the two collective bands start from the 12^+ and 20^+ states in experiment [17]. In Fig. 7, we compare alignments of the experimental positive-parity bands in ^{192}Os and the CNSB (CNS + pairing) $(+, 0)(+, 0)$ yrast configuration with a prolate ($-30^\circ < \gamma < 0^\circ$) and triaxial ($\gamma \approx -90^\circ$) shape. Observations from the experimental yrast sequence reveal two distinct and abrupt increases in angular momentum. These increments occur at approximately $I \approx 12^+$ and $I \approx 20^+$ states, corresponding to alignment gains of approximately $12\hbar$ and $8\hbar$, respectively, mentioned in Ref. [17]. Similar alignment gain is also observed in the main sequence of the isotones ^{194}Pt and ^{196}Hg [47], see Fig. 3 of Ref. [17]. As depicted in the present Fig. 3, the yrast line is initially constructed upon a collective prolate configuration up to around $I = 10$. Then subsequently it undergoes a transition into a triaxial state. With this in mind, we have drawn a dashed line between the alignment curve of the prolate and triaxial configurations around $I = 10$ in Fig. 7. When comparing the calculations with the experimental data, it becomes apparent a general agreement with alignments around $I = 12$ and $I = 20$. The greater sharpness in the theoretical alignments compared with the experimental results can likely be

attributed to the calculations being performed within a fixed deformation framework.

Upon examining the experiment and calculations presented in Fig. 6, it is evident that there is overall consistency at $I = 0-10$ for the ground state band, for the band built on the 12^+ isomer for $I = 12-18$ and then for the band which in experiment is built on the 20^+ state for $I = 22-26$. The calculated band for $I = 22-26$ is built on the $\pi(h_{11/2})^{-2}\nu(i_{13/2})^{-2}$ configuration where these high- j holes are almost fully aligned. Let us then consider a fixed deformation at an approximate calculated deformation of these $I = 22-26$ states, $\varepsilon_2 = 0.16$, $\varepsilon_4 = 0.03$, $\gamma = -85^\circ$. At this deformation at small rotational frequencies, the proton $h_{11/2}$ holes contribute with $\approx 9.5\hbar$ compared with their maximal values $10\hbar$ while the $i_{13/2}$ neutron holes contribute with $\approx 11.5\hbar$ compared with $12\hbar$. Thus, at this deformation, it is straightforward to build an $I = 22$ state from these almost fully aligned holes if a small contribution from the other particles is added, where this contribution is created at a small cranking frequency. As $I = 22$ is the maximum spin which can be created from the four holes alone, the $I = 22$ state can of course also be formed at axial symmetry, $\gamma = -120^\circ$, but this $I = 22$ state is calculated more than 0.5 MeV higher in energy than the $\gamma \approx -85^\circ$ state.

The question is then how the observed $I = 20$ state can be formed at the chosen deformation. In standard cranking calculations, only positive rotational frequencies are considered. This means that only positive contributions to the spin is possible from the core which is built from pairs of particles in the orbitals which are occupied. Therefore, because the four high- j holes contribute with $\approx 21\hbar$, it is not possible to form any $I = 20$ state from such standard cranking calculations. On the other hand, it should be possible to create an $I = 20$ state if the core spin is in the opposite direction. In the cranking formalism, such a core spin in the opposite direction could be formed at a negative cranking frequency. To our knowledge, such negative rotational frequencies have not been introduced in any cranking calculations. In any case, our interpretation is that the $I = 20^+$ isomer is formed with almost fully aligned high- j holes where a small negative contribution to the spin from the core particles makes it possible to form a state at a relatively low energy two spin units below full alignment of the high- j holes. Such isomers could in general be expected at high spin with several aligned high- j holes (or particles).

Recent evidence has been presented supporting the existence of a collective 12^+ isomer in ^{194}Os [48]. However, there is currently no evidence supporting the observation of long-lived 12^+ state in other Os isotopes that are predicted by theory, although studies demonstrate the systematic observation of long-lived 12^+ states in Pt ($Z = 78$) isotopes with $N = 112-120$ [19,24]. In the present study, we are motivated to investigate the existence of a 12^+ neutron state in $N = 116$ isotones, systematically. We delve into this further in the next section.

V. COLLECTIVE AND NONCOLLECTIVE STATES IN $N = 116$ ISOTONES

Taking a closer examination of single-neutron energies, as illustrated in Fig. 1(b), reveals two fundamental 2-qn configu-

rations as the primary components of potential isomers within the mass region characterized by $Z = 72-80$ and $N = 116$:

- (1) 10^- : $\nu 11/2[615]9/2[505]$ which has a noncollective structure with $\gamma = -120^\circ$;
- (2) 12^+ : $\nu 13/2[606]11/2[615]$ which has a collective structure with $\gamma \approx -90^\circ$.

It is important to note that the noncollective 10^- state is expected to have a $\Delta I = 1$ band built on it, while the 12^+ is collective, with an expected $\Delta I = 2$ band. For the $N = 116$ isotones, we have systematically investigated configurations that utilize these specific components as fundamental building blocks, as summarized in Table II. Our calculations suggest that the ground state in the studied nuclei is prolate ($\gamma \approx 0^\circ$) from ^{188}Hf to ^{193}Ir . Then we move through the γ -soft region at ^{194}Pt and the region of oblate-prolate shape coexistence at ^{195}Au .

Just as the 8^- 2-qn isomers are significant in the $N = 106$ isotones [49], the 10^- intrinsic state defines a sequence in the formation of a favored prolate noncollective state in the $N = 116$ isotones. Within Table II, we have depicted the configuration of these candidate isomers, which arise from the coupling of the proton configuration (including 0^+ for even-even isotones) with the 10^- neutron-core structure, spanning the proton numbers $Z = 72-79$. As discussed in Sec. III, it is evident that the 10^- neutron structure exhibits a noncollective prolate deformation. This characteristic is well known experimentally in the isomers of ^{190}W and ^{192}Os , with half-lives of 166 μs and 5.9 s, respectively [46]. Notably, our present calculations successfully reproduce these isomers with a prolate shape, $\gamma = -120^\circ$. In this current study, we predict the presence of a 10^- isomer in the neutron-rich and unstable Hf isotope, ^{188}Hf , with an energy of 1.304 MeV, representing the lowest excitation energy within the scope of the considered isotones. Our investigation has delved further into the prediction of isomeric states within ^{188}Hf . Our calculations predict the presence of an 8^- proton isomer with an energy 1.691 MeV, which is a well-established K -magic number in $Z = 72$ Hf isotopes, and a 4-quasiparticle 18^+ isomer with an energy of 3.049 MeV, which is built from a combination of $7/2[404]9/2[514]$ proton structure and $11/2[615]9/2[505]$ neutron structure. Our findings are consistent with those presented in Ref. [50], where the configuration-constrained PES calculations predict the 18^+ isomer as the most favored state within the hafnium isotopic chain. The CNSB calculations (with standard single-particle parameters) as well as the configuration-constrained PES calculations have also predicted the existence of such 10^- and 18^+ isomers in ^{186}Hf [10,50]. It seems likely that there will be multiquasiparticle isomers in $^{186,188}\text{Hf}$ that are sufficiently long-lived to beta decay, and may be longer lived than their respective ground states.

Our calculations also indicate the presence of a favored 10^- state in ^{194}Pt with an excitation energy of approximately 2 MeV. Notably, among platinum isotopes, experimental evidence of the 10^- isomer has been observed in both ^{190}Pt and ^{192}Pt , with energies measured at 2.297 and 2.172 MeV, respectively [46]. Given this systematic trend, the existence

TABLE II. The energy, deformation and structure of two most favored states in $N = 116$ isotones. Note that the deformation is triaxial for the states associated with the 12^+ isomer, which means that the asymptotic labels are highly approximate. The experimental data are taken from Refs. [45,46].

Nucleus	K^π	E_{expt}	E_{theor}	ε_2	γ	ε_4	Proton conf.
Noncollective 11/2[615]9/2[505] neutron state							
$^{188}_{72}\text{Hf}_{116}$	10^-		1.304	0.18	-120°	0.055	GS
$^{189}_{73}\text{Ta}_{116}$	$25/2^-$		1.335	0.17	-120°	0.053	5/2[402]
$^{189}_{73}\text{Ta}_{116}$	$29/2^+$		1.439	0.17	-120°	0.056	9/2[514]
$^{190}_{74}\text{W}_{116}$	10^-	1.839	1.435	0.17	-120°	0.055	GS
$^{191}_{75}\text{Re}_{116}$	$25/2^-$	1.601	1.362	0.17	-120°	0.058	5/2[402]
$^{191}_{75}\text{Re}_{116}$	$29/2^+$		1.427	0.17	-120°	0.054	9/2[514]
$^{192}_{76}\text{Os}_{116}$	10^-	2.015	1.538	0.16	-120°	0.059	GS
$^{193}_{77}\text{Ir}_{116}$	$31/2^+$	2.277	1.684	0.15	-120°	0.052	11/2[505]
$^{194}_{78}\text{Pt}_{116}$	10^-		2.019	0.15	-120°	0.050	GS
$^{195}_{79}\text{Au}_{116}$	$31/2^+$	2.461+X	2.843	0.12	-80°	0.019	11/2[505]
Collective 13/2[606]11/2[615] neutron state							
$^{188}_{72}\text{Hf}_{116}$	12^+		1.822	0.16	-87°	0.023	GS
$^{189}_{73}\text{Ta}_{116}$	$25/2^+$		1.873	0.16	-89°	0.024	1/2[411]
$^{189}_{73}\text{Ta}_{116}$	$33/2^-$		2.039	0.16	-88°	0.023	9/2[514]
$^{190}_{74}\text{W}_{116}$	12^+	2.655	2.002	0.15	-89°	0.026	GS
$^{191}_{75}\text{Re}_{116}$	$25/2^+$		1.855	0.15	-88°	0.026	1/2[411]
$^{191}_{75}\text{Re}_{116}$	$33/2^-$		2.178	0.15	-94°	0.028	9/2[514]
$^{192}_{76}\text{Os}_{116}$	12^+	2.865	2.151	0.15	-92°	0.026	GS
$^{193}_{77}\text{Ir}_{116}$	$35/2^-$		1.875	0.14	-94°	0.024	11/2[505]
$^{193}_{77}\text{Ir}_{116}$	$27/2^+$		2.025	0.14	-90°	0.028	3/2[402]
$^{193}_{77}\text{Ir}_{116}$	$33/2^-$		2.471	0.14	-88°	0.020	9/2[514]
$^{194}_{78}\text{Pt}_{116}$	12^+	2.451	1.733	0.13	-88°	0.021	GS
$^{195}_{79}\text{Au}_{116}$	$27/2^+$		1.879	0.13	-86°	0.019	3/2[402]
$^{195}_{79}\text{Au}_{116}$	$25/2^+$	1.980	1.953	0.13	-84°	0.019	1/2[411]
$^{195}_{79}\text{Au}_{116}$	$35/2^-$		2.056	0.13	-84°	0.024	11/2[505]
$^{196}_{80}\text{Hg}_{116}$	12^+	2.439	1.902	0.12	-80°	0.017	GS

of a 10^- isomer in ^{194}Pt is highly anticipated. In view of the variety of experiments already performed for ^{194}Pt [45], it can be tentatively suggested that a millisecond isomer might have eluded observation.

In the isotones with odd proton number, the spin contribution originating from the last proton will be slightly questionable in constructing a favored state. The 73rd proton of ^{189}Ta is predicted to occupy either the 5/2[402] or 9/2[514] orbitals, contributing to the formation of either a $25/2^-$ or $29/2^+$ high- K isomeric state in the present calculations. Experimental observations in ^{191}Re have revealed the existence of three isomers with $I = 21/2^+$, $25/2^-$, and $23/2^+$ [51]. Our calculations have identified favored states with the $25/2^-$ and $29/2^+$ spins, featuring a noncollective structure and building on the 10^- neutron state. These states are formed through the coupling of a 5/2[402] proton configuration and a 9/2[514] proton configuration, respectively, with the underlying 10^- neutron-core structure. The $5/2^+$ and $9/2^-$ states are the lowest excited states in ^{191}Re with the energy 97 and 145 keV, respectively [45] that aligns with our findings. In our

calculations, we did not identify any $21/2^+$ and $23/2^+$ states associated with the aligned 10^- neutron state.

In both ^{193}Ir and ^{195}Au , the coupling of the 11/2[505] proton configuration with the 10^- neutron structure leads to the formation of the favored $31/2^+$ state. However, there is a distinction between these two nuclei: in ^{193}Ir , our calculations indicate a prolate shape for the $31/2^+$ state, while in ^{195}Au , the same state exhibits a triaxial shape with $\gamma \approx -80^\circ$. Upon further examination of the deformation of the $\pi 11/2[505]$ state, it becomes evident that the discrepancy lies in the deformation of this state. Specifically, the 11/2[505] proton state resides in a prolate minimum ($\gamma = -120^\circ$) in ^{193}Ir , whereas in ^{195}Au , it is situated in a triaxial minimum with $\gamma \approx -85^\circ$. Consequently, the triaxiality in the proton structure dominates in the formation of the $31/2^+$ state in ^{195}Au . The calculations based on the TRS theory also indicate that the $\pi(h_{11/2})^{-1}$ bands in odd- A Au isotopes are likely to possess triaxial deformations [52]. In experiment, a $31/2^+$ isomer has been detected in ^{193}Ir with an energy of 2.277 MeV and a half-life of 125 μs [46]. However, in the case of ^{195}Au , there is some uncertainty

regarding the energy and parity of the $31/2$ isomer [53]. Considering the presence of the $I^\pi = 31/2^+$ isomer observed in both ^{193}Au [54] and ^{193}Ir , the isotope and the isotone of ^{195}Au , it is reasonable to anticipate the existence of a positive-parity $31/2$ isomer in ^{195}Au . Alternatively, if the parity of the $31/2$ isomer in ^{195}Au is negative, the suggested structure would involve $\pi 11/2[505]\nu 11/2[615]9/2[624]$, as proposed in Ref. [53]. However, the plausibility of such a structural configuration is questionable due to the significant distance of the $11/2[615]$ and $9/2[624]$ neutron orbitals from the Fermi level, see Fig. 1(b). Based on our calculations, we predict the presence of a positive-parity $31/2$ isomer in the nucleus ^{195}Au with the structure $\pi 11/2[505]\nu 11/2[615]9/2[505]$.

The next most favored state in $N = 116$ isotones corresponds to the 12^+ neutron-core structure, including the $i_{13/2}$ neutron alignment, combined with the $I_p = 0$ proton state for even proton number systems and the odd proton state for odd proton number systems. Referring to Sec. IV, the 12^+ state, formed by the collective $13/2[606]11/2[651]$ neutron configuration, exhibits a triaxial shape, which predominantly characterizes favored states associated with this neutron structure. As seen in Table II, we predict a collective 12^+ state in ^{188}Hf with a favored energy which is still not explored in experiment. In other even-even nuclei, ^{190}W , ^{192}Os , and ^{194}Pt , the experimental observation of the 12^+ state aligns well with the predictions of the current theoretical approach. The formation of a rotational band associated with these states substantiates their collective nature. The systematic trends suggest favored states by coupling the proton states $1/2[411]$, $3/2[402]$, $9/2[514]$, and $11/2[505]$ with the 12^+ neutron state in odd-even nuclei, as shown in Table II. All of these states exhibit an excitation energy of approximately 2 MeV, indicating their identical decoupled neutron state. The $35/2^-$ isomer is also predicted in TRS calculations for the nuclei ^{193}Ir and ^{195}Au [53], showing a structure similar to that found in the current calculations.

In the $N = 116$ isotone, ^{196}Hg with $Z = 80$, our calculations indicate an oblate shape for the ground state. Consequently, the yrast line predominantly consists of oblate structures, including the 10^- state, which exhibits a near-oblate shape with $\gamma \approx -75^\circ$. Our calculations reveal that the 10^- state in ^{196}Hg exhibits a different structure when compared with analogous states observed in other isotones, indicating that it does not originate from a full aligned 10^- state. However, in our calculations, the collective 12^+ state of ^{196}Hg maintains a similar structure to the 12^+ state found in other $N = 116$ isotones, built on the $i_{13/2}$ neutron alignment, as demonstrated in Table II. This 12^+ state is also observed in experiment [25].

VI. SUMMARY AND CONCLUSION

We have utilized both unpaired CNS and paired CNSB calculations to explore the structural properties of observed and potential isomers within the osmium $Z = 76$ isotopes and $N = 116$ isotones. Our computational analyses revealed the presence of preferred prolate and triaxial broken-pair structures in even-even osmium isotopes spanning $N = 112$ – 118 and the $N = 116$ isotones within the range of $Z = 72$ – 80 .

In ^{192}Os , a competition between prolate and triaxial configurations is evident at various spin states, see Fig. 3. The study of residual interactions within prolate structures reveals that only the 2-quasiparticle 7^- and 10^- states, along with the 4-quasiparticle 18^+ and 22^+ states, exhibit favorable couplings. Consequently, these states experience a reduction in energy, while other states with unfavorable coupling are pushed to higher energy. Analyzing the favored prolate states in other Os isotopes shows an increase in the energy of the 10^- and 18^+ states in ^{194}Os because of the filling of the $9/2[505]$ neutron orbital in the $N = 118$ system. However, it is noteworthy that our present work also predicts the existence of very low-lying, high- K isomers, specifically the 12^+ and 18^+ states as well as the 22^+ state. It highly recommends experimental investigations to explore these predicted isomers in Os isotopes further.

In ^{192}Os , collective isomers are observed at $I = 12^+$ and 20^+ . It appears that they are formed in connection with alignments of pairs of $i_{13/2}$ neutron holes and $h_{11/2}$ proton holes. Thus, the 12^+ state is built at $\gamma \approx -90^\circ$ from close to full alignment of the $i_{13/2}$ holes. However, in the vicinity of this deformation, the four high- j holes $\nu(i_{13/2})^{-2}\pi(h_{11/2})^{-2}$ contribute with around $I = 21\hbar$ which means that an $I = 20$ state cannot be formed in a conventional cranking calculation because it relies on positive contributions from the core. We propose the possibility of a core spin in the opposite direction, achievable through negative cranking frequencies. This perspective suggests that the 20^+ isomer arises from nearly complete alignment of the high- j holes complemented by a small negative spin contribution from the core particles. Our findings align with results obtained through TRS calculations [18] which indicate that the observed second alignment arises from $h_{11/2}$ protons rather than hf neutrons or from the second alignment within the $i_{13/2}$ neutrons. Furthermore, our calculations suggest the presence of triaxiality ($\gamma \approx -85^\circ$ to -90°) rather than oblate deformation for these collective bands.

The calculations indeed depict a significant transition in the nuclear shape, going from prolate shape to oblate-prolate shape coexistence and then oblate shape as we move from $Z = 72$ to $Z = 80$ in the $N = 116$ isotones. Additionally, the noncollective and collective structures are systematically investigated in these certain nuclei. The examination of $N = 116$ isotones reveals a systematic presence of potential isomeric states characterized by distinct features, including noncollective 10^- ($\gamma = -120^\circ$) and collective 12^+ ($\gamma \approx -90^\circ$) states. These states are constructed upon the foundation of $11/2[615]9/2[505]$ and $13/2[606]11/2[615]$ neutron configurations, respectively. We have also compared the calculated excitation energies of these predicted isomers with available experimental data, and found good agreements between the two. Predicted but as-yet-unobserved isomers should be accessible in future experiments, which may be able to provide further insights into the complex and coexisting structures in this shape-transitional region.

ACKNOWLEDGMENT

We would like to thank Dr. Gillis Carlsson for useful discussions. This work was funded in part by Grant No. ST/V001108/1 from the UK STFC.

- [1] A. K. Jain, B. Maheshwari, and A. Goel, *Nuclear Isomers* (Springer, Singapore, 2022).
- [2] P. M. Walker and J. J. Carroll, *Phys. Today* **58**(6), 39 (2005).
- [3] P. M. Walker and Z. Podolyák, Nuclear Isomers, in *Handbook of Nuclear Physics*, edited by I. Tanihata, H. Toki, and T. Kajino (Springer, Singapore, 2023).
- [4] P. M. Walker and G. D. Dracoulis, *Nature (London)* **399**, 35 (1999).
- [5] A. Bohr and B. R. Mottelson, *Phys. Rev.* **90**, 717 (1953).
- [6] Y. Sun, J. Y. Zhang, and M. Guidry, *Phys. Rev. Lett.* **78**, 2321 (1997).
- [7] Y. Sun, X. R. Zhou, G. L. Long, E. G. Zhao, and P. M. Walker, *Phys. Lett. B* **589**, 83 (2004).
- [8] P. M. Walker and F. R. Xu, *Phys. Lett. B* **635**, 286 (2006).
- [9] S. Åberg, *Nucl. Phys. A* **306**, 89 (1978).
- [10] F. Amirzadeh, A. Kardan, P. M. Walker, and H.-L. Ma, *Phys. Rev. C* **102**, 034319 (2020).
- [11] K. Heyde and J. L. Wood, *Rev. Mod. Phys.* **83**, 1467 (2011).
- [12] G. D. Dracoulis, P. M. Walker, and F. G. Kondev, *Rep. Prog. Phys.* **79**, 076301 (2016).
- [13] M. G. Mayer and J. H. D. Jensen, *Elementary Theory of Nuclear Shell Structure* (Wiley, New York, 1955).
- [14] F. G. Kondev, G. D. Dracoulis, and T. Kibedi, *At. Data Nucl. Data Tables* **103–104**, 50 (2015).
- [15] R. R. Hilton and H. J. Mang, *Phys. Rev. Lett.* **43**, 1979 (1979).
- [16] U. S. Tandel, S. K. Tandel, P. Chowdhury, D. Cline, C. Y. Wu, M. P. Carpenter, R. V. F. Janssens, T. L. Khoo, T. Lauritsen, C. J. Lister, D. Seweryniak, and S. Zhu, *Phys. Rev. Lett.* **101**, 182503 (2008).
- [17] G. D. Dracoulis, G. J. Lane, A. P. Byrne, H. Watanabe, R. O. Hughes, F. G. Kondev, M. Carpenter, R. V. F. Janssens, T. Lauritsen, C. J. Lister *et al.*, *Phys. Lett. B* **720**, 330 (2013).
- [18] G. D. Dracoulis, *Phys. Scr.* **2013**, 014015 (2013).
- [19] S. K. Tandel, S. G. Wahid, P. Chowdhury, R. V. F. Janssens, M. P. Carpenter, T. L. Khoo, F. G. Kondev, T. Lauritsen, C. J. Lister, D. Seweryniak, and S. Zhu, *Phys. Lett. B* **750**, 225 (2015).
- [20] P. D. Stevenson, M. P. Brine, Zs. Podolyak, P. H. Regan, P. M. Walker, and J. R. Stone, *Phys. Rev. C* **72**, 047303 (2005).
- [21] P. Sarriguren, R. Rodriguez-Guzman, and L. M. Robledo, *Phys. Rev. C* **77**, 064322 (2008).
- [22] R. Fossion, D. Bonatsos, and G. A. Lalazissis, *Phys. Rev. C* **73**, 044310 (2006).
- [23] K. Nomura, T. Otsuka, R. Rodriguez-Guzman, L. M. Robledo, and P. Sarriguren, *Phys. Rev. C* **84**, 054316 (2011).
- [24] S. G. Wahid, S. K. Tandel, P. Chowdhury, R. V. F. Janssens, M. P. Carpenter, T. L. Khoo, F. G. Kondev, T. Lauritsen, C. J. Lister, D. Seweryniak, and S. Zhu, *Phys. Rev. C* **92**, 054323 (2015).
- [25] A. I. Levon, Yu. V. Nosenko, V. A. Onischuk, A. A. Schevchuk, and A. E. Stuchbery, *Nucl. Phys. A* **764**, 24 (2006).
- [26] G. D. Dracoulis, G. J. Lane, A. P. Byrne, H. Watanabe, R. O. Hughes, N. Palalani, F. G. Kondev, M. Carpenter, R. V. F. Janssens, and T. Lauritsen, *Phys. Lett. B* **709**, 59 (2012).
- [27] T. Bengtsson and I. Ragnarsson, *Nucl. Phys. A* **436**, 14 (1985).
- [28] B. G. Carlsson and I. Ragnarsson, *Phys. Rev. C* **74**, 011302(R) (2006).
- [29] T. Bengtsson, *Nucl. Phys. A* **496**, 56 (1989).
- [30] B. G. Carlsson, I. Ragnarsson, R. Bengtsson, E. O. Lieder, R. M. Lieder, and A. A. Pasternak, *Phys. Rev. C* **78**, 034316 (2008).
- [31] H.-L. Ma, B. G. Carlsson, I. Ragnarsson, and H. Ryde, *Phys. Rev. C* **90**, 014316 (2014).
- [32] K. Pomorski and J. Dudek, *Phys. Rev. C* **67**, 044316 (2003).
- [33] V. M. Strutinsky, *Nucl. Phys. A* **122**, 1 (1968).
- [34] P. Ring and P. Schuck, *The Nuclear Many-Body Problem* (Springer, New York, 2000).
- [35] A. Kardan, I. Ragnarsson, H. Miri-Hakimabad, and L. Rafat-Motevali, *Phys. Rev. C* **86**, 014309 (2012).
- [36] T. Bengtsson, *Nucl. Phys. A* **512**, 124 (1990).
- [37] S. Pilat, K. Pomorski, and A. Staszczak, *Z. Phys. A - Atom. Nucl.* **332**, 259 (1989).
- [38] H. Taheri, A. Kardan, and M. H. Hadizadeh Yazdi, *Phys. Rev. C* **98**, 054313 (2018).
- [39] K. Jain, P. M. Walker, and N. Rowley, *Phys. Lett. B* **322**, 27 (1994).
- [40] K. Jain, O. Burglin, G. D. Dracoulis, B. Fabricius, N. Rowley, and P. M. Walker, *Nucl. Phys. A* **591**, 61 (1995).
- [41] C. J. Gallagher and S. A. Moszkowski, *Phys. Rev.* **111**, 1282 (1958).
- [42] C. J. Gallagher, *Phys. Rev.* **126**, 1525 (1962).
- [43] C. Wheldon, J. Garcés Narro, C. J. Pearson, P. H. Regan, Zs. Podolyák, D. D. Warner, P. Fallon, A. O. Macchiavelli, and M. Cromaz, *Phys. Rev. C* **63**, 011304(R) (2000).
- [44] P. R. John, V. Modamio, J. J. Valiente-Dobón, D. Mengoni, S. Lunardi, T. R. Rodriguez, D. Bazzacco, A. Gadea, C. Wheldon, T. Alexander *et al.*, *Phys. Rev. C* **90**, 021301(R) (2014).
- [45] Nudat database, <https://www.nndc.bnl.gov/nudat3>
- [46] S. Garg, B. Maheshwari, B. Singh, Y. Sun, A. Goel, and A. K. Jain, *At. Data Nucl. Data Tables* **150**, 101546 (2023).
- [47] D. Mehta, Y. K. Agarwal, K. P. Blume, S. Heppner, H. Hübel, M. Murzel, K. Theine, W. Gast, G. Hebbinghaus, R. M. Lieder, and W. Urban, *Z. Phys. A: Hadrons Nucl.* **339**, 317 (1991).
- [48] G. D. Dracoulis, G. J. Lane, A. P. Byrne, H. Watanabe, R. O. Hughes, F. G. Kondev, M. P. Carpenter, R. V. F. Janssens, T. Lauritsen, C. J. Lister, D. Seweryniak, S. Zhu, P. Chowdhury, Y. Shi, and F. R. Xu, *EPJ Web Conf.* **66**, 02033 (2014).
- [49] G. D. Dracoulis, G. J. Lane, F. G. Kondev, A. P. Byrne, R. O. Hughes, P. Nieminen, H. Watanabe, M. P. Carpenter, R. V. F. Janssens, T. Lauritsen *et al.*, *Phys. Lett. B* **635**, 200 (2006).
- [50] H. L. Liu, F. R. Xu, P. M. Walker, and C. A. Bertulani, *Phys. Rev. C* **83**, 067303 (2011).
- [51] M. W. Reed, G. J. Lane, G. D. Dracoulis, F. G. Kondev, M. P. Carpenter, P. Chowdhury, S. S. Hota, R. O. Hughes, R. V. F. Janssens, T. Lauritsen *et al.*, *Phys. Lett. B* **752**, 311 (2016).
- [52] S. C. Wang, X. H. Zhou, Y. D. Fang, Y. H. Zhang, N. T. Zhang, B. S. Gao, M. L. Liu, J. G. Wang, F. Ma, Y. X. Guo *et al.*, *Phys. Rev. C* **85**, 027301 (2012).
- [53] G. D. Dracoulis, G. J. Lane, H. Watanabe, R. O. Hughes, N. Palalani, F. G. Kondev, M. P. Carpenter, R. V. F. Janssens, T. Lauritsen, C. J. Lister *et al.*, *Phys. Rev. C* **87**, 014326 (2013).
- [54] Y. Gono, R. M. Lieder, M. Müller-Veggian, A. Neskakis, and C. Mayer-Böricke, *Nucl. Phys. A* **327**, 269 (1979).